IEEE Photonics Journal
An IEEE Photonics Society Publication

Open Access

A Gradient Grating Period Guided-Mode Resonance Spectrometer

Volume 10, Number 1, February 2018

Hsin-Yun Hsu
Yi-Hsuan Lan
Cheng-Sheng Huang

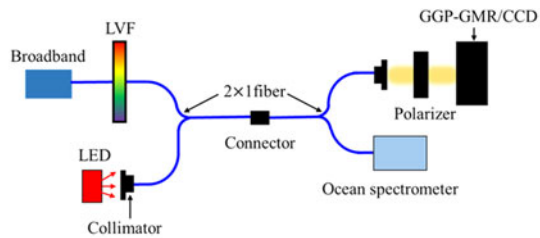

Reconstruction of dual input light sources with GGP-GMR spectrometer.

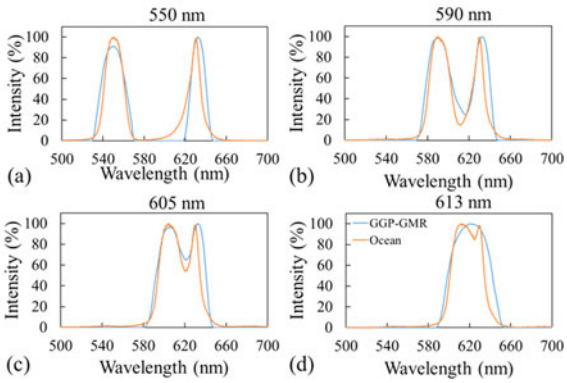

Reconstructed spectra from GGP-GMR and Ocean spectrometers.

DOI: 10.1109/JPHOT.2018.2793894
1943-0655 © 2018 IEEE

A Gradient Grating Period Guided-Mode Resonance Spectrometer

Hsin-Yun Hsu, Yi-Hsuan Lan, and Cheng-Sheng Huang

Department of Mechanical Engineering, National Chiao Tung University, Hsinchu 30010, Taiwan

DOI:10.1109/JPHOT.2018.2793894

Manuscript received December 13, 2017; accepted January 11, 2018. Date of publication January 15, 2018; date of current version February 8, 2018. This work was supported by the Ministry of Science and Technology in Taiwan under Grant 104-2633-E-009-001-MY2 and Grant 106-2221-E-009-120. Corresponding author: Cheng-Sheng Huang (e-mail: csh@nctu.edu.tw).

Abstract: This paper reports a compact spectrometer based on a guided-mode resonance (GMR) filter mounted on a linear charge-coupled device (CCD). The GMR is specially designed to exhibit gradient grating periods (GPPs) laterally to ensure that the GMR functions as a linear-variable bandstop filter. Each period corresponds to a resonant wavelength such that this wavelength is reflected back at its corresponding resonant period and transmitted to all other periods. Consequently, when a resonant wavelength is incident on the GGP-GMR attached to a linear CCD, the CCD pixel underneath its resonant period receives the minimum intensity, and the other pixels receive higher intensities. In terms of the wavelength range of interest, by scanning a single wavelength at a time, a transmission efficiency matrix that contains the transmission efficiency of each wavelength at each pixel can be established. An unknown incident spectrum can be reconstructed using the established transmission efficiency matrix and the intensity measured using the CCD. In this study, a GGP-GMR spectrometer less than 3 mm long that can achieve a wavelength detection range of 200 nm was demonstrated to reconstruct various incident spectra, including a single wavelength of light with a resolution of 0.5 nm, a single wavelength of light with varying intensity levels, and dual incident light sources.

Index Terms: Gratings, optical filters, spectroscopy, subwavelength structures, wavelength measurement.

1. Introduction

Spectrometers are vital for many applications such as color measurement [1], food quality control [2], [3], air and water monitoring [4]–[6], and biosensing [7]–[9]. A spectrometer can be used as a sensor by itself or as a detection instrument. Through the interaction between light and matter, when a light source is incident on a sample, its transmission or reflection can be recorded and analyzed using a spectrometer to determine the presence and quantity of a specific substance, for example, the use of absorption spectrometry for gas sensing [10] or food monitoring [2], [11]. A spectrometer can also be used as a detection instrument to measure the output spectral response of another sensor that is used to interact with the sample. For example, a spectrometer is often used to monitor the shift of the resonant wavelength from optical biosensors [12]–[14] caused by changes in the concentrations of adsorbed biomolecules.

Currently, the most commonly used spectrometers are based on diffraction gratings or prisms. By increasing the distance between the dispersive elements and the detection element for better

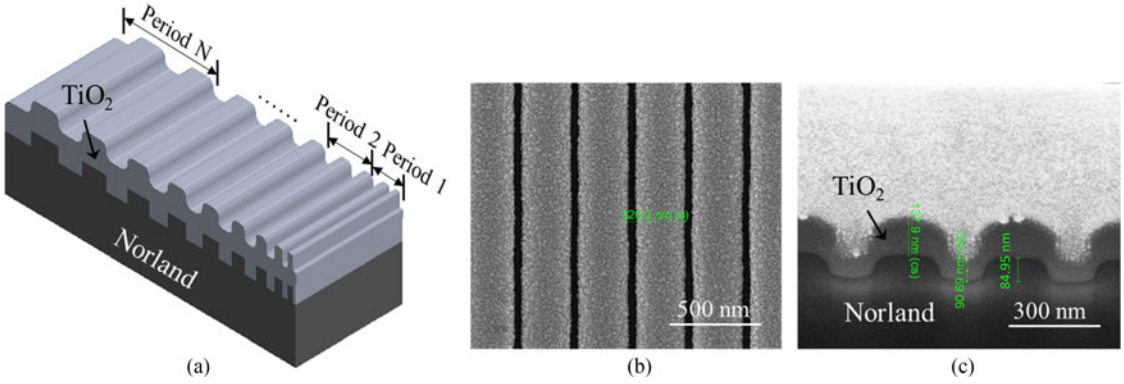

Fig. 1. (a) Schematic of GGP-GMR. (b) SEM image of the top view with a grating period of 320 nm. (c) SEM images of cross-sectional views. The replicated grating height is 85 nm on the Norland 68 and the thickness of TiO_2 is 91 and 138 nm in valley and peak of the grating, respectively.

wavelength discrimination, we can achieve impressive resolutions with these spectrometers. However, owing to the increasing demand for lab-on-a-chip (LOC), point-of-care and portable devices, and potential integration with smartphones, there is a strong demand for further miniaturization of compact spectrometers [15], [16]. Many compact spectrometers intended for potential on-chip integration and based on different mechanisms have been proposed and demonstrated, including photonic crystals [17], microdonut resonators [18], Fabry–Perot interferometers [19], [20], and quantum dots [16]. Recently, our group designed and fabricated a gradient grating period guided-mode resonance (GGP-GMR) filter [21] and demonstrated its potential for use as a compact spectrometer [22], where the spectra of monochromatic light and commercial LED light were successfully reconstructed. In this study, we further investigated the impact of resonance linewidth on the spectral resolution. Also we successfully demonstrated the ability of the proposed device to reconstruct the incident spectra with same wavelength but different intensities, which potentially can be applied for fluorescence intensity measurement. Lastly, we demonstrated the ability of GGP-GMR spectrometer to reconstruct more complex spectrum from two light sources and discussed the potential improvement on a GGP-GMR spectrometer.

2. Design, Fabrication, and Characterization

The central part of the GGP-GMR is the GMR filter, which functions as a bandstop filter. The resonance phenomenon of GMR filter has been studied theoretically and experimentally [23]–[25]. With appropriate design of the grating geometry and selection of materials, at normal incidence with a broadband light source, a specific wavelength of light (resonant wavelength) is reflected, and the rest of the light is transmitted through. The resonant wavelength can be calculated based on the second-order Bragg condition [26], $\lambda_R = n_{eff}\,\Lambda$. Here λ_R is the resonant wavelength, n_{eff} is the effective refractive index (RI), and Λ is the grating period. The effective refractive index can be considered as a weighted average of RIs of the GMR structure where the resonant mode is generated at resonant condition. The explicit formulation on how to calculate effective RI can be found in [27].

The resonance is very sensitive to the geometry of GMR filter including grating period, height and duty cycle, and thickness of waveguiding layer [28], and to the RIs of the GMR filter. Different designs have been demonstrated to realize wavelength-tunable GMR filters, including variable grating periods [29], [30], and variable waveguiding thicknesses [31], [32]. Recently, we demonstrated a gradient grating period GMR fabricated by electron beam lithography and replica molding [21]. By varying the grating period, as shown in Fig. 1(a), the GMR provides gradient resonance along the device, which is referred to as the GGP-GMR in this paper.

The fabrication of the GGP-GMR involved the following steps. First, a silicon master with a gradient grating pattern with periods ranging from 250 to 550 nm in 2-nm increments and a grating depth

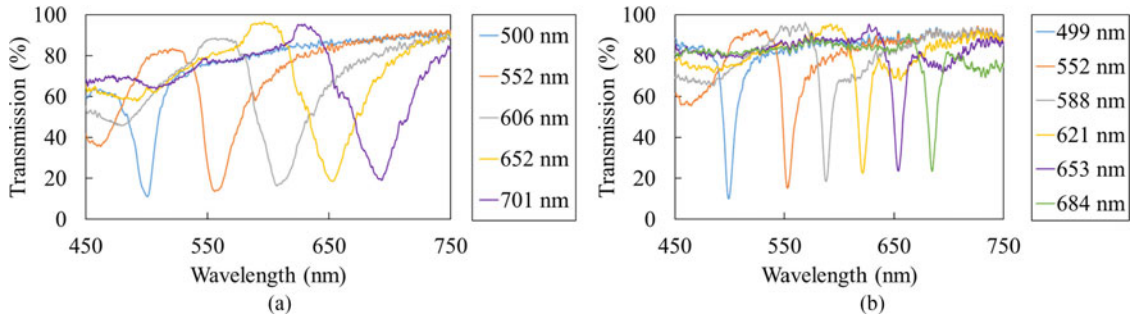

Fig. 2. Transmission spectra at different locations (or periods) of GGP-GMR for (a) TE and (b) TM polarization. The legends indicate the resonant wavelengths.

of 85 nm was fabricated through electron beam lithography and reactive ion etching. In this work, each period consists of 100 cycles resulting the whole device is only 6.04 mm. Next, the replica molding process was used to transfer the gradient grating pattern to a UV adhesive (Norland 68) on a polyethylene terephthalate sheet. Finally, a layer of TiO_2 was sputtered on top of Norland 68 to complete the process. Due to replica molding, the resulting GGP-GMR structure as illustrated in Fig. 1(a) forms double-grating waveguide structures with a grating under and above the waveguiding layer [33], [34]. The duty cyle of the resulting GGP-GMR increases with increasing of the grating period. For the purpose of this work, this has little effect on the GGP-GMR spectrometer. The detailed discussion on the fabricated GGP-GMR's geometry can be found in previous publication [21]. Scanning electron microscopy (SEM) images of the top and cross-sectional views of the GGP-GMR at periods of 302 nm with duty cycle $\sim$0.83 and 362 nm with duty cycle $\sim$0.7 are presented in Fig. 1(b) and (c), respectively, which indicate successful replication of the grating pattern on Norland 68.

Based on previous study [21], the GGP-GMR with grating periods from 250 to 550 nm can have resonant wavelength over 400 nm depending on the polarization, thickness of TiO_2, and grating depth. For the purpose of this work, we only used the grating regions that can support resonant wavelengths between 500 to 700 nm for the demonstration of its use as a spectrometer. A transmission setup was used to characterize the transmission characteristics of the GGP-GMR. An optical fiber (P50-2-VIS-NIR, Ocean Optics) with a core having a diameter of 50 μm connected to a broadband light source (LS-1-LL, Ocean Optics) was used to illuminate at different locations (or periods) of the GGP-GMR in close proximity without collimation, and the transmitted light was either transverse-electric (TE)- or transverse-magnetic (TM) polarized before it was collected by another fiber, which was connected to a commercial spectrometer (USB2000+VIS-NIR-ES, Ocean Optics), referred to as Ocean spectrometer in this paper. Fig. 2 presents the transmission spectra corresponding to both TE and TM polarization with resonant wavelengths of approximately 500–700 nm, which is the required wavelength range for the subsequent spectral reconstruction.

According to the transmission measurement, TE polarization exhibits marginally high coupling efficiency–lower transmission efficiency at resonant wavelengths. The full width at half maximum (FWHM) of TM resonance is significantly narrower than that of TE resonance. The FWHM of TM polarization varies from 10 to 14 nm, whereas that of TE polarization can be as broad as 55 nm. The broader linewidth from TE resonance can be attributed to better mode confinement [23]. The broader FHWM of the resonance can have a large impact on the spectral resolution, as discussed in a later section.

3. Data Processing

To realize a spectrometer, the GGP-GMR was attached to a linear CCD (LHCCD01304 ToupTek) with a pixel size of 8 $\times$ 200 μm. Given a spectral range of interest, we can digitalize it into N channels, and the intensity of each channel is denoted by I_j ($j = 1 \ldots N$). N detectors from corresponding

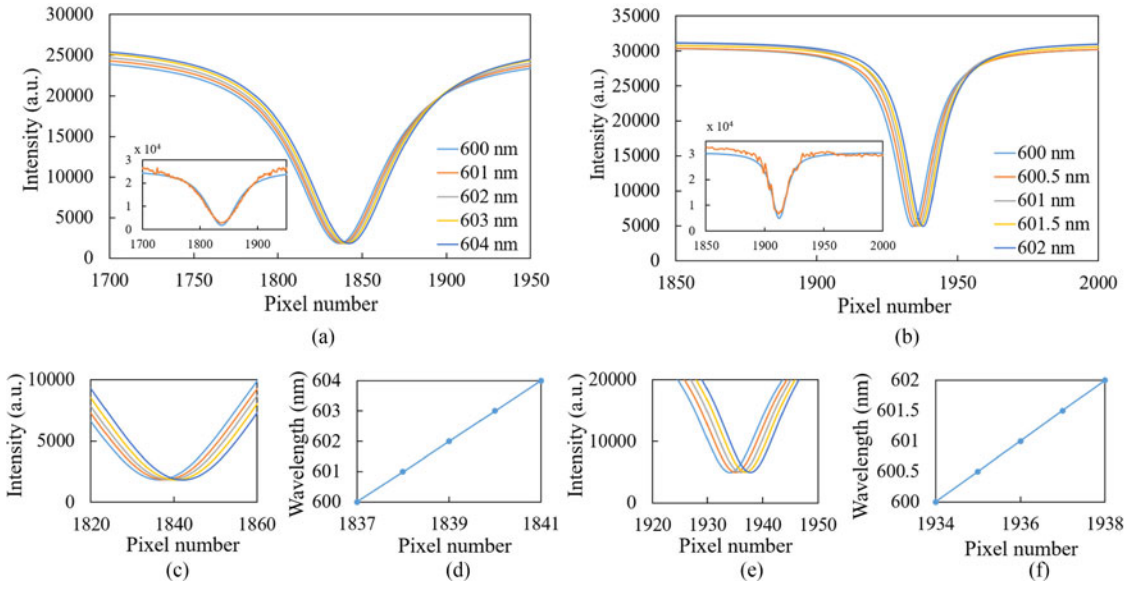

Fig. 3. Intensity distribution of a linear CCD for (a) TE and (b) TM polarizations. (c) and (e) Closeups of the minimum intensity regions for TE and TM polarization, respectively. (d) and (f) Relationship between resonant wavelength and pixels for TE and TM polarizations, respectively.

pixels were also selected, and the intensity measured by these pixels is denoted by C_j ($j = 1 \ldots N$). When a specific wavelength, I_j, is incident on a linear CCD with the attached GGP-GMR, such light resonates at a specific grating period of the GGP-GMR. Therefore, this light is reflected back from the location, and the pixel underneath exhibits the minimum intensity. By contrast, this wavelength of light is transmitted in all other periods of the GGP-GMR; hence, the pixels behinds all these periods exhibit high intensities. Therefore, for a specific incident wavelength, I_j, the intensity distribution on the CCD exhibits dip characteristics; the pixel corresponding to the minimum intensity is selected as the wavelength-corresponding detector, C_j.

Each detector exhibits a characteristic wavelength-dependent efficiency due to the GGP-GMR. The relationship between an input spectrum, I_j, and output intensity, C_j, can be expressed as $C = TI$, where T is a transmission efficiency matrix, and each element, T_{ij} ($i, j = 1 \ldots N$), represents the transmission efficiency at a specific detector (pixel) for a specific wavelength channel, which can be experimentally obtained.

For an unknown incident spectrum, I_j ($j = 1 \ldots N$), based on the intensity measured at the detectors (pixels) C_j ($j = 1 \ldots N$) and precalibrated T matrix, the original spectrum I_j can be calculated or reconstructed. In this study, we used the fmincon function from the nonlinear optimization toolbox in MATLAB to calculate the incident spectrum.

4. Results and Discussion

4.1 Impact of Polarization

The GMR is polarization-dependent, hence, the selection of TE or TM can be crucial for certain applications. In this study, we first investigated the resonance characteristics of the linear CCD for both TE and TM polarization. A monochromator (DK242, Spectral Products) was used to scan wavelengths of 1 and 0.5 nm for TE and TM resonance, respectively. As discussed in the previous section, each wavelength has a corresponding pixel with the minimum intensity, which is selected as Cj. To more accurately determine the pixel corresponding to the minimum intensity, a Lorentzian function suggested by Ganesh *et al.* [35] was used to fit the original intensity distribution of the CCD. Fig. 3(a) and (b) present the fitted intensity distributions for TE and TM polarization for five

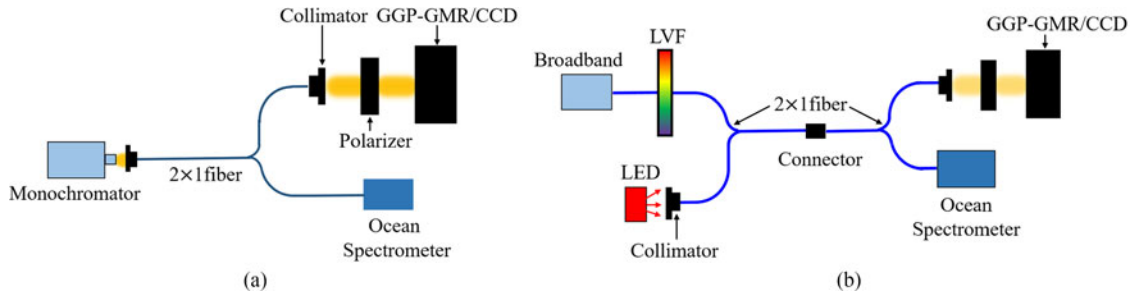

Fig. 4. Experimental setup for spectral reconstruction of (a) single wavelength and (b) dual input light sources. LVF stands for linear variable filter.

different wavelengths. The original intensity profiles of 601 and 600.5 nm for TE and TM polarization with the corresponding fitted curves were also shown in the insets of Fig. 3(a) and (b), respectively. Fig. 3(c) and (e) present zoomed-in images of the pixels with the minimum intensity, and Fig. 3(d) and (f) present the relationship between the pixel corresponding to the minimum intensity and the incident wavelength.

Because of different effective refractive indices for different polarizations, the same wavelength resonates at different periods, resulting in the minimum intensity at different pixels, as shown in Fig. 3(a) and (b). The coupling efficiency at the resonant pixel for the resonant wavelength is defined as the ratio of intensity difference between the nonresonant region and the resonant pixel to the intensity in the nonresonant region, and its values were 0.92 and 0.83 for TE and TM polarization, respectively. The FWHM in terms of number of pixels for TE was 64 pixels, which is four times the value for TM (16 pixels). This result is consistent with the transmission measurement shown in Fig. 2. For TE polarization, the GGP-GMR achieved 1 nm/pixel as shown in Fig. 3(d); by contrast, 0.5 nm/pixel can be achieved with TM polarization due to its narrower FWHM as indicated in Fig. 3(f). In brief, with a narrower FWHM, the GGP-GMR can achieve better resolution in single-wavelength detection.

4.2 Demonstration of Spectral Reconstruction

To verify the proposed GGP-GMR spectrometer, two different light sources were used: single-wavelength light from a monochromator and dual input light sources with the experimental setup, as shown in Fig. 4(a) and (b), respectively. For the reconstruction of the single-wavelength light, the light generated from a monochromator was coupled into a 1 $\times$ 2 fiber. One end was incident on the Ocean spectrometer, and the other end was allowed to pass through a polarizer before it was incident on the GGP-GMR/CCD. To obtain a higher spectral resolution, TM polarization was used in this study, as discussed in the Impact of polarization section. Two different scenarios were tested for single-wavelength demonstration: different wavelengths with the same intensity and same wavelength with different intensities.

4.2.1 Different Wavelengths With Same Intensity: Five different wavelengths with a separation of 0.5 nm generated from the monochromator were TM polarized and directly illuminated on the GGP-GMR. Based on the intensities measured at the CCD pixels Cj and the precalibrated transmission efficiency matrix T, the incident spectra were then calculated according to the discussion in the data processing section. Fig. 5(a) shows the reconstructed spectra. The inset is the close-up of the peaks, indicating that the GGP-GMR spectrometer can accurately reconstruct the spectra of wavelengths separated by 0.5 nm. The FWHM slightly varied between 2.22 and 2.78 nm, which is comparable to that measured using the Ocean spectrometer ($\sim$2.48 nm). The intensity variation between wavelengths was within 7%.

4.2.2 Same Wavelength With Different Intensities: We fixed the incident wavelength at 600 nm but varied the intensity at four different levels according to the settings of the monochromator. Fig. 5(b) shows the reconstructed spectra at four different levels from the GGP-GMR spectrometer,

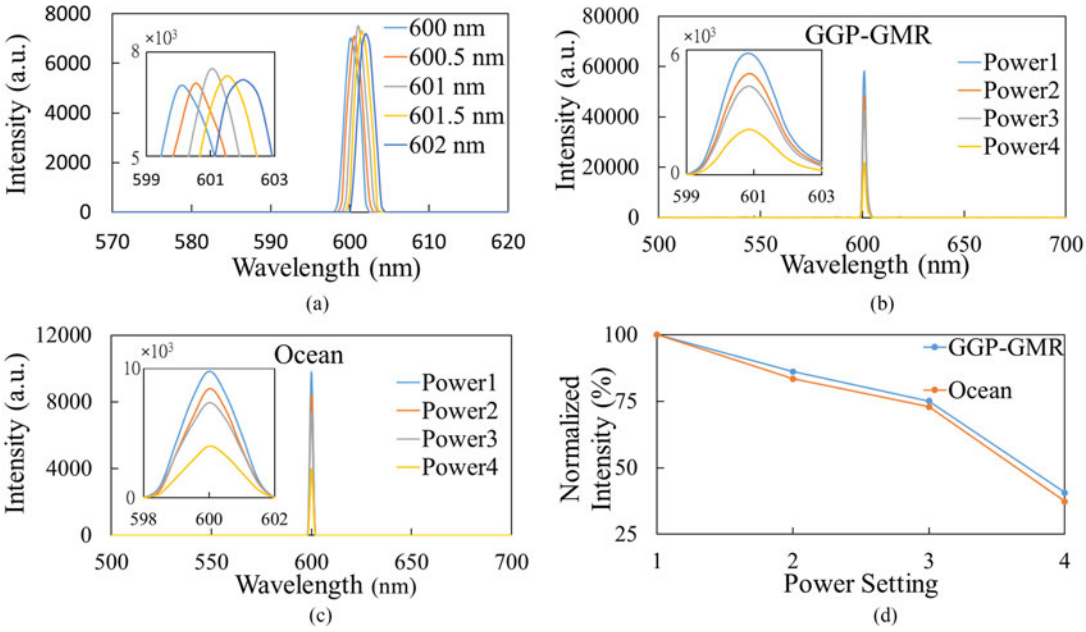

Fig. 5. (a) Reconstructed spectra of five different single wavelengths separated by 0.5 nm. (b) and (c) Reconstructed spectra of 600 nm at different power settings by using the GGP-GMR and the ocean spectrometer, respectively. (d) Normalized intensity measured using both the GGP-GMR and the ocean spectrometer.

and the inset shows a close-up of the peaks with different aspect ratio in x and y axes from original figures for better visualization of peaks. The spectra measured using the Ocean spectrometer are also shown in Fig. 5(c) for comparison. For each case, by normalizing the intensities against the maximum intensity (Power 1), the intensities measured using the GGP-GMR exhibited a very similar trend to those measured using the Ocean spectrometer (Fig. 5(d)). Successful demonstration of this experiment implies the potential applications such as fluorescence measurement where the intensity of the florophores' emission peak wavelength can be correlated to the concentration of target biomolecules.

4.2.3 Dual Input Light Sources: We further demonstrated spectral reconstruction by combining two different light sources (Fig. 4(b)), one from a commercial red LED and the other from a broadband light source passing through a linear variable filter (LVF, Ocean Optics Product Inc.), which allows us to control the center wavelength. The combined light was again passed through a 1×2 fiber, where one end was incident on the Ocean spectrometer and the other on the GGP-GMR spectrometer. In this study, the center wavelength of the red LED was fixed, and we adjusted the LVF such that its center wavelength shifted toward that of the red LED. Thus, we adjusted the center wavelength of the LVF at 550, 589, 605, and 613 nm based on the Ocean spectrometer. The reconstructed spectra are shown in Fig. 6; the intensity was normalized against the intensity of the red LED. The orange and blue curves represent the spectra measured using the Ocean and the GGP-GMR spectrometers, respectively. When these two peaks were further apart, the wavelength detection results obtained using the GGP-GMR were fairly close to those obtained using the Ocean spectrometer.

Table 1 summarizes the wavelengths of the two peaks and the relative intensities obtained in four different experiments. The center wavelengths of the LVF measured using the GGP-GMR and the Ocean spectrometer were nearly same. The variation was only 0.096%, 0.017%, and 0.048% for (a), (b), and (c), respectively, from Table 1. By contrast, the center wavelength of the red LED, as measured using the GGP-GMR, was constant at 632.5 nm; however, that measured using the Ocean spectrometer was 630.0 nm. This result could be because the Ocean spectrometer and monochromator were not calibrated. We are currently investigating strategies to mitigate this

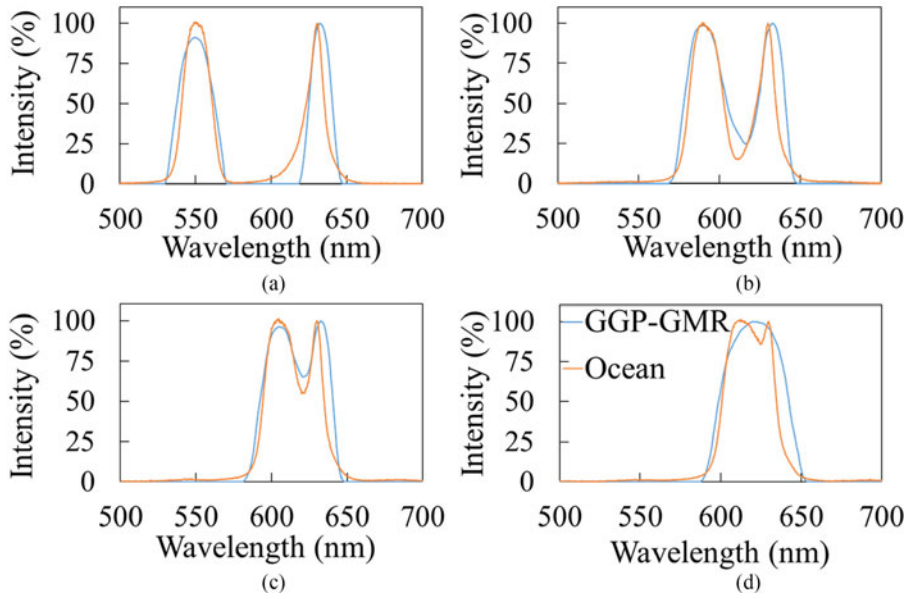

Fig. 6. Reconstructed spectra of four different center wavelengths from LVF. (a) 550, (b) 589, (c) 605, and (d) 613 nm.

TABLE 1
Summary of Peak Wavelength and Relative Intensity Measured Using GGP-GMR and Ocean Spectrometers

	GGP-GMR			Ocean		
	LVF		LED	LVF		LED
	Peak	Intensity	Peak	Peak	Intensity	Peak
(a)	549.5	91.1	632.5	550.0	100.9	630.6
(b)	589.5	98.8	632.5	589.4	100.4	629.9
(c)	605.0	96.5	632.5	604.7	101.3	629.9
(d)	620.0	100.0	620.0	613.0	101.2	629.6

Unit: Peak [nm]; Intensity [%].

problem. In terms of intensity, the GGP-GMR obtained a higher intensity from the LED than from the LVF. By contrast, the Ocean spectrometer obtained a higher intensity from the LVF. The largest intensity variation was 9.7% in case (a). This can possibly be ascribed to slight differences in ambient lighting conditions compared with those during measurement of the transmission efficiency matrix.

When the two peaks were too close to each other (Fig. 6(d)), the GGP-GMR spectrometer failed to resolve them; instead, a single peak at 620 nm was obtained. However, the Ocean spectrometer could detect the two peaks—613.03 and 629.58 nm. To consider the resolution of the GGP-GMR spectrometer more carefully, we examined the intensity distributions on the linear CCD corresponding to Fig. 6(c) and (d). Two dips were observed around pixels 1926 and 1980 (Fig. 7(a)), and these were caused by the two center peaks of the LVF and LED. When these two peaks were too close

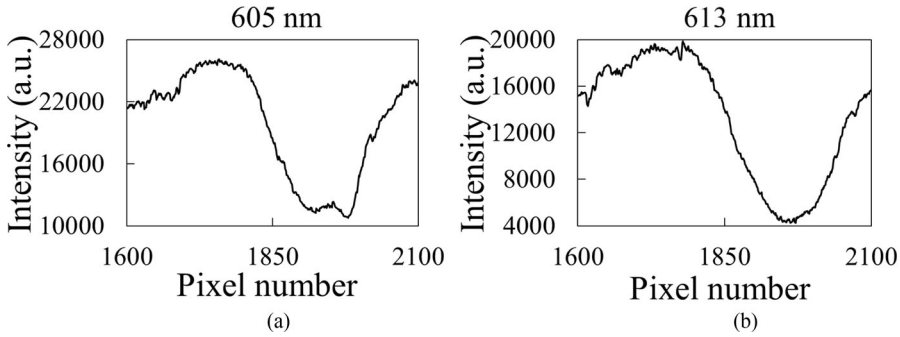

Fig. 7. (a) and (b) Intensity distributions on CCD corresponding to Fig. 6(c) and (d), respectively.

to each other (Fig. 6(d)), the intensity distribution at the linear CCD failed to resolve them; instead, these two dips merged into a single large dip (Fig. 7(b)), which leads to difficulty in reconstructing the original spectrum by using the existing algorithm. As suggested by Bao [7], a more sophisticated reconstruction algorithm might be required to improve the reconstruction accuracy. Alternatively, a higher quality factor of the resonance from the GGP-GMR can also more efficiently preserve these dips in the intensity distribution of the linear CCD for subsequent spectral reconstruction.

5. Conclusion

In this paper, we presented a GGP-GMR spectrometer system that is less than 3 mm long and with a wavelength detection range of 200 nm. We performed spectral reconstruction by using two different types of light sources. For single-wavelength light, the GGP-GMR accurately detected the peak wavelength with a resolution of 0.5 nm. For the same single-wavelength light with different intensities, the GGP-GMR spectrometer accurately measured the relative intensity levels. Moreover, we successfully demonstrated the reconstruction capability of the GGP-GMR spectrometer for dual input lights, when the center wavelength of the two incident lights was greater than 16.6 nm. Despite slight variations in the relative intensity levels between the two peaks and the center peak wavelength, further research is warranted to optimize performance. The GGP-GMR spectrometer represents a new paradigm for high-resolution spectral measurement in a compact configuration, and it can be used for further miniaturization of detection systems, such as lab-on-a-chip systems and handheld devices.

Acknowledgment

The authors thank the Nano Facility Center at National Chiao Tung University and National Nano Device Laboratories, Taiwan, for their support in the fabrication and characterization of the GGP-GMR. This manuscript was edited by Wallace Academic Editing.

References

[1] S. Johnsen, "How to measure color using spectrometers and calibrated photographs," *J. Exp. Biol.*, vol. 219, no. 6, pp. 772–778, Mar. 2016.
[2] V. A. McGlone, R. B. Jordan, and P. J. Martinsen, "Vis/NIR estimation at harvest of pre- and post-storage quality indices for 'Royal Gala' apple," *Postharvest Biol. Technol.*, vol. 25, no. 2, pp. 135–144, Jun. 2002.
[3] H. Lin *et al.*, "Effective variables selection in eggs freshness graphically oriented local multivariate analysis using NIR spectroscopy," in *Proc. Int. Conf. Chem., Mater. Food Eng.*, 2015, pp. 13–18.
[4] D. Degler *et al.*, "Extending the toolbox for gas sensor research: Operando UV/vis diffuse reflectance spectroscopy on SnO2-based gas sensors," *Sens. Actuators B, Chem.*, vol. 224, pp. 256–259, Mar. 2016.
[5] S. Dutta, D. Sarma, and P. Nath, "Ground and river water quality monitoring using a smartphone-based pH sensor," *AIP Adv.*, vol. 5, May 2015, Art. no. 057151.
[6] Y. T. Hu *et al.*, "Detection of water quality multi-parameters in seawater based on UV-Vis spectrometry," in *Proc. Oceans 2016, Shanghai*, 2016, pp. 1–4.

[7] J. S. Yuk *et al.*, "Analysis of protein arrays with a dual-function SPR biosensor composed of surface plasmon microscopy and SPR spectroscopy based on white light," *Sens. Actuators B, Chem.*, vol. 129, no. 1, pp. 113–119, Jan. 2008.
[8] Y. Wang *et al.*, "Smartphone spectrometer for colorimetric biosensing," *Analyst*, vol. 141, no. 11, pp. 3233–3238, 2016.
[9] X. L. Xu *et al.*, "A simple, fast, label-free colorimetric method for detection of telomerase activity in urine by using hemin-graphene conjugates," *Biosens. Bioelectron.*, vol. 87, pp. 600–606, Jan. 2017.
[10] X. Liu *et al.*, "A survey on gas sensing technology," *Sensors*, vol. 12, no. 7, pp. 9635–9665, Jul. 2012.
[11] H. K. Lichtenthaler and C. Buschmann, "Chlorophylls and carotenoids: Measurement and characterization by UV-VIS spectroscopy," in *Current Protocols in Food Analytical Chemistry*. Hoboken, NJ, USA: Wiley, 2001.
[12] Y. K. Tu *et al.*, "Integration of a guided-mode resonance filter with microposts for in-cell protein detection," *Analyst*, vol. 141, no. 13, pp. 4189–4195, 2016.
[13] M. G. Scullion, T. F. Krauss, and A. Di Falco, "Slotted photonic crystal sensors," *Sensors*, vol. 13, no. 3, pp. 3675–3710, Mar. 2013.
[14] D. Wawro *et al.*, "Optical fiber endface biosensor based on resonances in dielectric waveguide gratings," *Proc. SPIE*, vol. 3911, pp. 86–94, 2000.
[15] B. Redding *et al.*, "Compact spectrometer based on a disordered photonic chip," *Nature Photon.*, vol. 7, no. 9, pp. 746–751, Sep. 2013.
[16] J. Bao and M. G. Bawendi, "A colloidal quantum dot spectrometer," *Nature*, vol. 523, no. 7558, pp. 67–70, Jul. 2015.
[17] N. K. Pervez *et al.*, "Photonic crystal spectrometer," *Opt. Exp.*, vol. 18, no. 8, pp. 8277–8285, Apr. 12, 2010.
[18] Z. X. Xia *et al.*, "High resolution on-chip spectroscopy based on miniaturized microdonut resonators," *Opt. Exp.*, vol. 19, no. 13, pp. 12356–12364, Jun. 2011.
[19] S. W. Wang *et al.*, "Concept of a high-resolution miniature spectrometer using an integrated filter array," *Opt. Lett.*, vol. 32, no. 6, pp. 632–634, Mar. 2007.
[20] A. Emadi *et al.*, "Design and implementation of a sub-nm resolution microspectrometer based on a linear-variable optical filter," *Opt. Exp.*, vol. 20, no. 1, pp. 489–507, Jan. 2, 2012.
[21] H. A. Lin and C. S. Huang, "Linear variable filter based on a gradient grating period guided-mode resonance filter," *IEEE Photon. Technol. Lett.*, vol. 28, no. 9, pp. 1042–1045, May 2016.
[22] H. A. Lin *et al.*, "Compact spectrometer system based on a gradient grating period guided-mode resonance filter," *Opt. Exp.*, vol. 24, no. 10, pp. 10972–10979, May 2016.
[23] S. S. Wang and R. Magnusson, "Theory and applications of guided-mode resonance filters," *Appl. Opt.*, vol. 32, no. 14, pp. 2606–2613, May 1993.
[24] S. S. Wang and R. Magnusson, "Design of wave-guide-grating filters with symmetrical line-shapes and low side-band," *Opt. Lett.*, vol. 19, no. 12, pp. 919–921, Jun. 1994.
[25] A. Sharon, D. Rosenblatt, and A. A. Friesem, "Resonant grating waveguide structures for visible and near-infrared radiation," *J. Opt. Soc. Amer. A, Opt. Image Sci. Vision*, vol. 14, no. 11, pp. 2985–2993, Nov. 1997.
[26] R. Magnusson *et al.*, "Photonic devices enabled by waveguide-mode resonance effects in periodically modulated films," *Proc. SPIE*, vol. 5225, pp. 20–34, 2003.
[27] I. D. Block *et al.*, "Sensitivity model for predicting photonic crystal biosensor performance," *IEEE Sens. J.*, vol. 8, nos. 3/4, pp. 274–280, Mar./Apr. 2008.
[28] J. Ju, Y.-A. Han, and S.-M. Kim, "Design optimization of structural parameters for highly sensitive photonic crystal label-free biosensors," *Sensors*, vol. 13, no. 3, pp. 3232–3241, Mar. 2013.
[29] F. Bruckner *et al.*, "Widely tunable monolithic narrowband grating filter for near-infrared radiation," *Opt. Lett.*, vol. 36, no. 4, pp. 436–438, Feb. 2011.
[30] C. L. Fang *et al.*, "Tunable guided-mode resonance filter with a gradient grating period fabricated by casting a stretched PDMS grating wedge," *Opt. Lett.*, vol. 41, no. 22, pp. 5302–5305, Nov. 2016.
[31] L. Y. Qian *et al.*, "Tunable guided-mode resonant filter with wedged waveguide layer fabricated by masked ion beam etching," *Opt. Lett.*, vol. 41, no. 5, pp. 982–985, Mar. 2016.
[32] D. W. Dobbs, I. Gershkovich, and B. T. Cunningham, "Fabrication of a graded-wavelength guided-mode resonance filter photonic crystal," *Appl. Phys. Lett.*, vol. 89, Sep. 18, 2006, Art. no. 123113.
[33] C. Kappel *et al.*, "Resonant double-grating waveguide structures as inverted Fabry-Perot interferometers," *J. Opt. Soc. Amer. B, Opt. Phys.*, vol. 21, no. 6, pp. 1127–1136, Jun. 2004.
[34] O. Stenzel *et al.*, "Observation of the waveguide resonance in a periodically patterned high refractive index broadband antireflection coating," *Appl. Opt.*, vol. 53, no. 14, pp. 3147–3156, May 2014.
[35] N. Ganesh *et al.*, "Compact wavelength detection system incorporating a guided-mode resonance filter," *Appl. Phys. Lett.*, vol. 90, Feb. 19, 2007, Art. no. 081103.